Superratio and the simple ratios of π^+ and π^- elastic scattering on ^{3}H and ^{3}He at 180 MeV to investigate charge symmetry

B. M. K. Nefkens, W. J. Briscoe,* A. D. Eichon,† D. H. Fitzgerald,‡
A. Mokhtari,* and J. A. Wightman§
Department of Physics, University of California at Los Angeles, Los Angeles, California 90024

M. E. Sadler
Department of Physics, Abilene Christian University, Abilene, Texas 79699
(Received 14 December 1989)

Results are presented for the charge-symmetry superratio R, simple ratios r_1 and r_2, and the differential cross sections of π^+ and* π^- elastic scattering on ^{3}H and ^{3}He: $R=r_1r_2$, $r_1=\sigma(\theta)[\pi^+\,^3\mathrm{H}\to\pi^+\,^3\mathrm{H}]/\sigma(\theta)[\pi^-\,^3\mathrm{He}\to\pi^-\,^3\mathrm{He}]$, and $r_2=\sigma(\theta)[\pi^-\,^3\mathrm{H}\to\pi^-\,^3\mathrm{H}]/\sigma(\theta)[\pi^+\,^3\mathrm{He}\to\pi^+\,^3\mathrm{He}]$. The measurements were made at $T_\pi=180$ MeV and $\theta_\pi(\mathrm{lab})=40°-90°$; some data were obtained at $T_\pi=143$ MeV also. At all angles, $R>1$ and $r_2>1$ indicative of a violation of charge symmetry; however, we also find that $r_1\simeq1$. Our data are consistent with $F_p(^3\mathrm{H})\simeq F_n(^3\mathrm{He})$ and $F_n(^3\mathrm{H})>F_p(^3\mathrm{He})$, where F_p and F_n are the proton and neutron matter form factors. $\sigma(\theta)[\pi^\pm\,^3\mathrm{H}\to\pi^\pm\,^3\mathrm{H}]$ decreases with increasing magnitude of the four-momentum transfer t up to $\theta_{\mathrm{c.m.}}\simeq70°$; the t dependence of the F's is comparable to that of the electromagnetic form factors. $\sigma(\theta)[\pi^-\,^3\mathrm{H}\to\pi^-\,^3\mathrm{H}]$ has a non-spin-flip dip at $\theta_{\mathrm{c.m.}}\simeq78°$.

I. INTRODUCTION

Charge symmetry (CS) plays an important role in nuclear physics.[1,2] It explains the equality of the cross sections of charge-symmetric reactions such as

$$\sigma(\theta)[p\,^3\mathrm{H}\to p\,^3\mathrm{H}]=\sigma(\theta)[n\,^3\mathrm{He}\to n\,^3\mathrm{He}]\ ,$$

the fore-aft symmetry of the differential cross section and polarization of isomirror reactions such as $d+\alpha\to{}^3\mathrm{He}+{}^3\mathrm{H}$, and the identical spin-parity values of excited states of mirror nuclei such as ^{11}B and ^{11}C. In its original form, CS was defined as the equality of the nn and pp interactions. In general, CS is the invariance of a system under the isomirror operator $\hat{P}_{\mathrm{CS}}$, which reverses the sign of the third component of isospin I_3. The isomirror operator rotates a system by π about the I_2 axis in isospin space, $\hat{P}_{\mathrm{CS}}\equiv\exp(i\pi\hat{I}_2)$. Technically, when CS is valid $\hat{P}_{\mathrm{CS}}$ commutes with the Hamiltonian $\hat{H}$ or $[\hat{H},\hat{P}_{\mathrm{CS}}]=0$. Protons are subject to Coulomb repulsion, but neutrons are not, therefore $\sigma(\theta)[pp\to pp]$ is not exactly equal to $\sigma(\theta)[nn\to nn]$, and CS cannot be strictly valid. For many years it was believed that charge-symmetry breaking (CSB) was due only to electromagnetic (em) interactions. But a pure em violation proved to be incapable of explaining the data on isospin-multiplet mass splittings and meson mixings. Thus, nuclear charge-symmetry breaking (NCSB) became an important subject. In the one-boson exchange models of the nucleon-nucleon interaction, NCSB is occurring dynamically via $\rho^0-\omega$ and $\pi^0-\eta$ mixing.[3]

The modern era in CSB began when the quark model and quantum chromodynamics (QCD) were applied. Instead of the charge-symmetry operator being a certain rotation in an abstract isospin space, it is now the interchange of the up and down quarks,

$$\hat{P}_{\mathrm{CS}}|\mathrm{up}\rangle=|\mathrm{down}\rangle$$

and

$$\hat{P}_{\mathrm{CS}}|\mathrm{down}\rangle=-|\mathrm{up}\rangle\ .$$

This definition makes it possible to give a concrete meaning to CSB, namely all the consequences of the up-down quark interchange. Thus, CSB is due to the differences between the light quarks which are the following.

(1) The mass differences $\Delta m=m_d-m_u$.

(2) The electromagnetic differences resulting from the different electric charges and magnetic moments of the quarks.

The QCD Lagrangian contains the quark-mass terms

$$-\bar{q}_u m_u q_u-\bar{q}_d m_d q_d+\cdots\ ,$$

where the q's are the relevant quark state functions (see Ref. 4 for details); such a Lagrangian manifestly violates charge symmetry when the quark masses are not identical. In the standard model, the strong interaction between quarks is flavor independent and approximate CS arises because the effect of the up-down quark-mass difference in the basic Lagrangian is small compared to that of the fundamental quark-quark interaction.[5]

The study of CSB is especially interesting because it is one of the rare, readily explorable effects of the quark structure of hadrons, specifically of the quark-mass difference. CSB manifests itself even at very low energies where QCD has otherwise little predictive power. Within

the framework of specific quark models, such as the cloudy bag model, one can quantitatively evaluate the CSB effects.[6] We have embarked on an extensive set of CSB experiments that involve interactions of pions with the one-, two-, and three-nucleon systems. The two CSB mechanisms, the mass difference and the electromagnetic differences, always act simultaneously but not with equal strength. We hope that the systematic study of systems which can be characterized by the interchange of one, two, or three up and down quarks will prove helpful in delineating CSB. For example, the comparison of the isomirror systems $\pi^+ {}^3\mathrm{H}$ and $\pi^- {}^3\mathrm{He}$ shows the effect of the interchange of one down with one up quark.

In this report, we present the final results of an investigation of CS in π^+ and π^- elastic scattering on the isospin doublet ^{3}H-^{3}He at $T_\pi = 180$ MeV from $\theta_{\mathrm{lab}} = 40°$ to 90°. Included are also some data obtained at $T_\pi = 143$ MeV from 40° to 70°. Preliminary results have already been published.[7] The choice of the three-nucleon system is particularly relevant if CSB is related to the three-body force.[8] There are good three-nucleon wave functions[9] available based on Faddeev equations to facilitate theoretical analyses.

Extensive treatises on CS and CSB are given in Refs. 1–3. A new classification of various tests of CS in systems with light nuclei, that is based on the up-down quark difference of the isomirror states, was introduced in Ref. 10. No other test of CS using pion interactions with the ^{3}H-^{3}He isospin doublet existed before this investigation except for the exploratory measurement at lower energies.[11]

CS implies that the following ratios are equal to one at every energy and angle:

$$r_1 \equiv \frac{\sigma(\theta)[\pi^+ {}^3\mathrm{H} \to \pi^+ {}^3\mathrm{H}]}{\sigma(\theta)[\pi^- {}^3\mathrm{He} \to \pi^- {}^3\mathrm{He}]} , \tag{1a}$$

$$r_2 \equiv \frac{\sigma(\theta)[\pi^- {}^3\mathrm{H} \to \pi^- {}^3\mathrm{H}]}{\sigma(\theta)[\pi^+ {}^3\mathrm{He} \to \pi^+ {}^3\mathrm{He}]} . \tag{1b}$$

We will refer to these as the simple ratios. Ideally, for the precise measurement of the absolute cross sections one would like to have intense π^+ and π^- beams that are very much alike; they are hard to find because π^+ is produced seven times more abundantly than π^-, also π^+ and π^- beams differ in proton and electron contaminations. The great difficulty is the determination of the intensity of the π^+ and π^- beams to high absolute accuracy as well as the efficiency of the pion detector. To avoid the uncertainties introduced by these experimental prerequisites, we have concentrated our efforts on a novel test of CS that is based on the measurement of the so-called superratio which we defined[7] as

$$R \equiv \frac{\sigma(\theta)[\pi^+ {}^3\mathrm{H}] \times \sigma(\theta)[\pi^- {}^3\mathrm{H}]}{\sigma(\theta)[\pi^+ {}^3\mathrm{He}] \times \sigma(\theta)[\pi^- {}^3\mathrm{He}]} = r_1 \times r_2 . \tag{2}$$

This ratio is obtained by measuring the two relative yields ρ_+ and ρ_- where

$$\rho_+ \equiv \frac{\mathrm{Yield}(\pi^+ {}^3\mathrm{H} \to \pi^+ {}^3\mathrm{H})}{\mathrm{Yield}(\pi^+ {}^3\mathrm{He} \to \pi^+ {}^3\mathrm{He})} \times \frac{N(^3\mathrm{He})}{N(^3\mathrm{H})} , \tag{3a}$$

$$\rho_- \equiv \frac{\mathrm{Yield}(\pi^- {}^3\mathrm{H} \to \pi^- {}^3\mathrm{H})}{\mathrm{Yield}(\pi^- {}^3\mathrm{He} \to \pi^- {}^3\mathrm{He})} \times \frac{N(^3\mathrm{He})}{N(^3\mathrm{H})} . \tag{3b}$$

$N(^3\mathrm{H})$ and $N(^3\mathrm{He})$ are the number of ^{3}H and ^{3}He atoms in the targets, respectively. Thus, we have $R = \rho_+ \times \rho_-$. The yield measurements require knowing neither the absolute π^+ and π^- beam intensities nor the detector efficiency and solid angle.

Besides the investigation of CS, there are some other interesting aspects of measuring π^+ and π^- elastic scattering on ^{3}H and ^{3}He. It has been suggested[11] that r_1 and r_2 provide a possible way for comparing the proton distribution in ^{3}H with the neutron distribution in ^{3}He as well as the neutron distribution in ^{3}H with the proton distribution in ^{3}He. This is of particular interest since elastic electron scattering is not sensitive to the wave function of the neutrons in ^{3}H where the two neutrons have antiparallel spins. Forward elastic electron scattering[12–14] yields the electric form factor which represents the proton distributions in ^{3}He and ^{3}H. Backward or magnetic scattering depends partly on the exchange currents and on the magnetic moment which is dominated by the distribution of the unpaired neutron in ^{3}He or by the proton distribution in ^{3}H. It has been suggested[15] that after taking into account multiple scattering and off-mass shell uncertainties, the proton matter form factor of ^{3}H can be inferred from a measurement of $\sigma(\theta)[\pi^+ {}^3\mathrm{H} \to \pi^+ {}^3\mathrm{H}]$ in the angular region $\theta_\pi \simeq 70°$. It can then be compared to the electromagnetic form factors derived from electron scattering.

The angular distribution for $\pi^+ {}^3\mathrm{H}$ elastic scattering up to about $\theta_{\mathrm{lab}} = 70°$ shows a smoothly decreasing cross section which has a similar slope as the charge and magnetic form factors of ^{3}H. The elastic scattering of π^- on tritium has a dip near $\theta_{\mathrm{lab}} = 70°$, which does not depend on incident energy. This dip is thus not a diffraction dip, rather it is the consequence of the spin-flip nature of π-N scattering near 90° in the πN c.m. system. Single spin flip is not allowed on the paired neutrons of ^{3}H, hence the name "non-spin-flip dip," or NSF dip.

In this paper we present data on the superratio, r_1, r_2, ρ_-, ρ_+, and $\pi^\pm$ elastic scattering cross sections; the latter are based on a calibration of EPICS using $\pi^\pm$ scattering data on hydrogen.[16] This will enable one to make quantitative tests of different models for the pion-trinucleon interaction.

II. EXPERIMENT AND ANALYSIS

The measurements were carried out using the EPICS facility at LAMPF. The beam energy at the center of the tritium target was 180 MeV; some data were taken at $T_\pi = 143$ MeV also. The momentum acceptance of the channel is ±1%. A 0.3-cm-thick graphite absorber in the π^+ beam was used to remove the protons. The same absorber is used in the π^- beam so as to have similar properties for the π^+ and π^- beams. The π^+ beam intensity is about seven times that of the π^- beam. At 40°, $T_\pi = 180$ MeV, the π^+ beam intensity was reduced with

the horizontal jaws upstream in order to keep the acquisition dead time less than 20%. The pion fluxes were monitored with an ionization chamber (IC) located in the evacuated EPICS scattering chamber about 85-cm downstream of the target ladder. The response of this IC depends on the beam contamination; the IC is not absolutely calibrated. At 50°, 70°, and 90°, the IC reading was found to have an increase of about 3% due to beam backscattering from the aluminum scattering chamber support that was in the beam at these angles. Another ionization chamber monitored the proton beam just before the pion production target. The ratio of these two ionization chambers was constant to better than 1.5% for most runs. Extensive checks of the relative monitoring were done using the pion-scattering yield from the steel containers of the tritium and ^{3}He targets. The consistency was good, typically better than 2% for the ^{3}H-^{3}He targets. To enable us to make an extra check on the relative beam monitoring at the forward-angle points, we added 25% deuterium to the ^{3}H and ^{3}He targets; this allows for a *simultaneous* measurement of π-*d* elastic scattering; there is sufficient kinematic separation between the ^{3}H and deuterium elastic scattering peaks for a clean measurement. At angles larger than 60°, our statistics on the πd scattering are not sufficient for a precision test.

We used gaseous targets in sealed containers mounted on a ladder located at the center of the EPICS scattering chamber. A target could be moved quickly in and out of the beam by remote control and the position of each target in the beam was readily reproducible. The gas containers were identical spheres made of stainless steel, 12-cm-diam, 0.06-cm wall thickness, they were copper clad and plated with a gold flash of a few angstroms to prevent tritium diffusion out of the containers. A thin filling tube was welded to the top of each sphere. The containers were filled at the Los Alamos National Laboratory (LANL) WX-5 facility using a system that included a mass spectrograph and pressure and temperature gauges for target density measurements. The filling lines were welded shut after the filling. At the conclusion of the experiment, the containers were emptied to check the gas density and composition using a special device for rupturing the filling line such that all gas was collected in a calibrated volume. The results for both tritium gas density measurements were consistents to 1% while ^{3}He was different by 2.4%. This caused an uncertainty in the ^{3}H/^{3}He gas ratio of 3% which is reflected in a 3% systematic uncertainty in r_1 and r_2 and 6% in R. The target contents were as follows: No. 1, 9.8 atm ^{3}H and 3.5 atm D_2; No. 2, 10.5 atm ^{3}He and 3.3 atm D_2; No. 3, 13.6 atm H_2; No. 4, evacuated. Near the end of the experiment, a fifth container was filled with 13.7 atm D_2 for a few measurements of πd elastic scattering. All containers were pressure tested extensively before use including x-ray and rupture tests. The amount of tritium in target No. 1 was 30 kCi. A special vent system for EPICS was installed, and there were tritium monitoring and alarm systems at critical places.

The EPICS spectrometer was used to measure the elastic scattering of π^+ and π^- at θ_π(lab)=40°–90°. At each angle we successively measured the π^+ yield from the tritium, ^{3}He and hydrogen targets with the spectrometer

TABLE I. The cross section ratios ρ_+ and ρ_-. The full angular bin θ is divided into two "half-bins" θ'.

θ_{lab}	$\theta^{\pi}_{c.m.}$ (±1.7°)	ρ_+	ρ_-	$\theta'^{\pi}_{c.m.}$ (±0.8°)	ρ_+	ρ_-
			At T_π=180 MeV			
40°	44.0°	0.692±0.014	1.56±0.04	42.5°	0.696±0.021	1.58±0.06
				45.5°	0.682±0.022	1.53±0.06
50°	54.7°	0.880±0.021	1.32±0.05	53.2°	0.858±0.030	1.41±0.08
				56.2°	0.950±0.036	1.20±0.07
60°	65.3°	1.37±0.04	0.909±0.053	63.8°	1.30±0.06	0.882±0.081
				66.8°	1.49±0.07	0.910±0.101
65°	70.5°	2.10±0.14		69.0°	2.08±0.21	
				72.0°	2.30±0.20	
70°	75.7°	2.58±0.12	0.496±0.027	74.2°	3.06±0.45	0.493±0.051
				77.2°	2.69±0.20	0.490±0.052
75°	80.9°	2.25±0.17		79.4°	2.75±0.40	
				82.4°	1.87±0.19	
80°	85.9°	1.36±0.07	0.829±0.057	84.4°	1.45±0.14	0.704±0.089
				87.4°	1.33±0.08	0.970±0.092
90°	96.0°	0.944±0.036	1.14±0.07	94.5°	0.939±0.057	1.00±0.09
				97.5°	0.944±0.054	1.27±0.12
			At T_π=143 MeV			
40°	43.6°	0.628±0.011	1.73±0.06			
50°	54.2°	0.711±0.019	1.47±0.05			
60°	64.7°	1.02±0.03				
70°	75.1°	1.55±0.12				

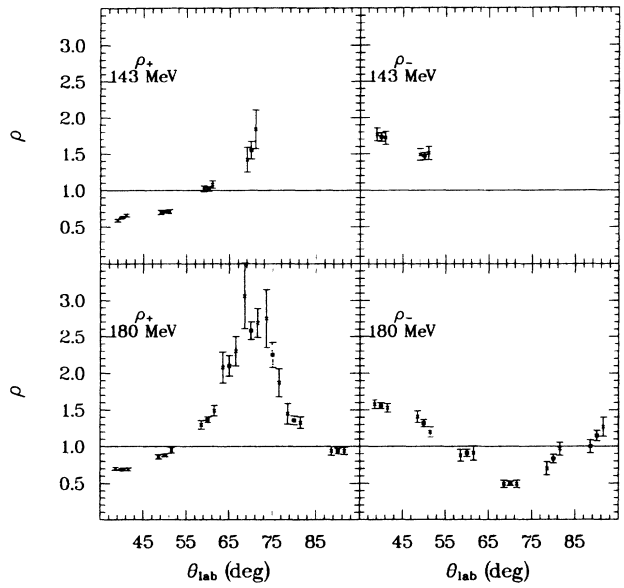

FIG. 1. ρ_+ and ρ_- at $T_\pi = 143$ and 180 MeV,

$$\rho_+ = \sigma(\theta)[\pi^+ {}^3\mathrm{H}]/\sigma(\theta)[\pi^+ {}^3\mathrm{He}] ,$$

$$\rho_- = \sigma(\theta)[\pi^- {}^3\mathrm{H}]/\sigma(\theta)[\pi^- {}^3\mathrm{He}] .$$

The squares indicate the full EPICS angular acceptance of 3.5°. The crosses indicate two adjacent minibins of 1.6°. The solid line at $\rho = 1$ is for reference purposes only.

tuned for pion-tritium elastic scattering kinematics yielding the ratio ρ_+ introduced in Eq. (3),

$$\rho_+ = \frac{Y(\pi^+ {}^3\mathrm{H} \to \pi^+ {}^3\mathrm{H}) - Y(\pi^+ bgd)}{Y(\pi^+ {}^3\mathrm{He} \to \pi^+ {}^3\mathrm{He}) - Y(\pi^+ bgd)} \times \frac{N({}^3\mathrm{He})}{N({}^3\mathrm{H})} , \tag{4a}$$

where the Y's are the normalized yields. For background measurements we used the hydrogen target. It was chosen because hydrogen and tritium have the same multiple scattering; the elastic scattering peak of hydrogen is sufficiently far away from the tritium peak so that the background subtraction can be done smoothly and reliably. The measurement of ρ_+ was followed immediately by a measurement of π^+ elastic scattering on hydrogen and the empty target with the spectrometer tuned for πp elastic kinematics. This enabled us to make a measurement of the pion flux and spectrometer acceptance which is needed to obtain the simple ratios r_1 and r_2 and to calculate the elastic scattering differential cross sections. This sequence was repeated for incident π^- to measure

$$\rho_- = \frac{Y(\pi^- {}^3\mathrm{H} \to \pi^- {}^3\mathrm{H}) - Y(\pi^- bgd)}{Y(\pi^- {}^3\mathrm{He} \to \pi^- {}^3\mathrm{He}) - Y(\pi^- bgd)} \times \frac{N({}^3\mathrm{He})}{N({}^3\mathrm{H})} . \tag{4b}$$

The live time of the data acquisition computer was always $> 75\%$.

The standard EPICS replay package was used; it includes software projections of the pion trajectory back to the scattering target for the elimination of a few events outside the acceptable parameter ranges. The program includes evaluations of the computer dead time and the efficiencies of the spectrometer chambers. The kinematics for each event were calculated and every event was histogrammed according to its pseudomissing mass T. The T histogram is used to evaluate the number of good events. In every set of four measurements that is needed to calculate the superratio, we used the same size bin in the four T histograms for the signal peak; we always checked that the peaks were exactly in the same location on the focal plane. When determining the absolute cross sections, care was taken that the bin size was not too small so that all scattered pions were included. The kinematic smearing is most serious for πp scattering leading to a rather broad peak and a correspondingly large background. Since the $\pi^- p$ signal is quite small, the largest uncertainty in the absolute cross section comes from the $\pi^- p$ measurement. The data were collected for the full angular acceptance of the EPICS spectrometer which is 3.5°. We used the software to divide this into two contiguous miniangular bins of $\sim 1.6°$ each.

III. RESULTS

The ρ's, given by Eq. (4) are equivalent to the ratios of the cross sections, thus,

$$\rho_+ = \frac{\sigma(\theta)[\pi^+ {}^3\mathrm{H} \to \pi^+ {}^3\mathrm{H}]}{\sigma(\theta)[\pi^+ {}^3\mathrm{He} \to \pi^+ {}^3\mathrm{He}]} \tag{5a}$$

and

$$\rho_- = \frac{\sigma(\theta)[\pi^- {}^3\mathrm{H} \to \pi^- {}^3\mathrm{H}]}{\sigma(\theta)[\pi^- {}^3\mathrm{He} \to \pi^- {}^3\mathrm{He}]} . \tag{5b}$$

The numerical results for the ρ_+ and ρ_- for the full 3.5° angular interval, as well as the two miniangular bins obtained in this experiment, are given in Table I and are shown in Fig. 1. The ρ's are our most precise data; the systematic error is $\pm 1.5\%$ and stems from the uncertainty in the $^3\mathrm{H}/^3\mathrm{He}$ gas pressure ratio. The numerical value of ρ depends strongly on the scattering angle, for example, in the region from 40° to 90°, ρ_+ changes from 0.7 to 2.8 and back to 0.9. This variation is due to the different angular dependencies of the spin-flip and non-spin-flip

TABLE II. The superratio R. Not included in the quoted error is the systematic error of $\pm 3\%$ in the ratio of the gas pressures.

θ_{lab}	$\theta_{\mathrm{c.m.}}$	R
	At $T_\pi = 180$ MeV	
40°	44.0°±1.7°	1.08±0.04
50°	54.7°	1.16±0.05
60°	65.3°	1.25±0.08
70°	75.7°	1.30±0.10
80°	85.9°	1.13±0.10
90°	96.0°	1.08±0.07
	At $T_\pi = 143$ MeV	
40°	43.6°±1.7°	1.09±0.04
50°	54.2°	1.04±0.05

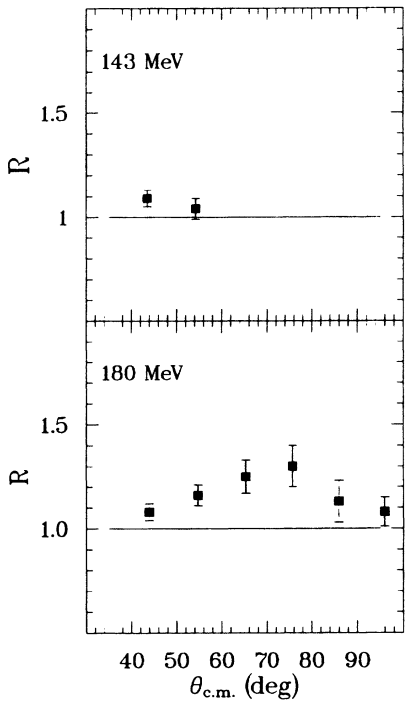

FIG. 2. The superratio at $T_\pi = 143$ and 180 MeV for the full angular bins,

$$R = \sigma(\theta)[\pi^+ {}^3\mathrm{H}] \cdot \sigma(\theta)[\pi^- {}^3\mathrm{H}] / \sigma(\theta)[\pi^- {}^3\mathrm{He}] \cdot \sigma(\theta)[\pi^+ {}^3\mathrm{He}] \, .$$

The solid line at $R = 1$ shows the expected ratio when CS is valid.

amplitudes as discussed in Sec. IV.

The results for the superratio R are given in Table II and shown in Fig. 2. The systematic error is ±3%, double the uncertainty in the gas pressure ratio. The CS prediction is $R = 1$. We see that R deviates from 1.0 at all angles. This deviation is evidence for a violation of charge symmetry, it will be discussed in Sec. IV.

The charge-symmetry simple ratios r_1 and r_2 are obtained from the relative yields and the known $\pi^\pm p$ scattering cross sections,

$$r_1 = \frac{Y(\pi^+ {}^3\mathrm{H})}{Y(\pi^- \mathrm{He})} \times \frac{Y(\pi^- p)}{Y(\pi^+ p)} \times \left\{ \frac{\sigma(\theta)[\pi^+ p]}{\sigma(\theta)[\pi^- p]} \right\}_{\mathrm{PWA}} , \quad (6)$$

and similarly for r_2. The numerical data for the $\sigma(\theta)[\pi^+ p]/\sigma(\theta)[\pi^- p]$ ratio come from the VPI SP 87 πN partial-wave analysis[16] (PWA). The results for r_1 and r_2 are given in Table III and shown in Fig. 3. The systematic error is a combination of the uncertainty in the ^{3}H/^{3}He gas pressure ratio and the relative π^+ and π^- beam calibration which is ±3%, giving a total systematic error of ±4%. The CS prediction is $r_1 = r_2 = 1$. The contributions to the uncertainties in r_1 and r_2 coming from the beam normalization error are negatively correlated while the gas pressure errors are positively correlated. It is seen from Fig. 3 that r_1 is nearly constant and close to the CS value of one, while r_2 deviates markedly from one implying that the CSB found in the superratio is mainly due to CSB in r_2 as discussed in Sec. IV.

TABLE III. The ratios r_1 and r_2. Not included in the quoted error is a ±1.5% error in the gas pressure ratio.

θ_{lab}	$\theta_{\mathrm{c.m}}$	r_1	r_2
	At $T_\pi = 180$ MeV		
40°	44.0°±1.7°	1.04±0.03	1.04±0.03
50°	54.7°	1.05±0.05	1.10±0.04
60°	65.3°	1.07±0.05	1.17±0.06
70°	75.7°	1.07±0.04	1.20±0.08
80°	85.9°	1.03±0.06	1.09±0.08
90°	96.0°	0.988±0.057	1.09±0.05
	At $T_\pi = 143$ MeV		
40°	43.6°±1.7°	1.04±0.05	1.04±0.04
50°	54.2°	1.02±0.08	1.01±0.08
60°	64.7°		1.13±0.08
70°	75.1°		1.11±0.15

The cross sections for π^+ elastic scattering on ^{3}H were obtained by normalization to $\pi^+ p$ elastic scattering

$$\sigma(\theta)[\pi^+ {}^3\mathrm{H} \to \pi^+ {}^3\mathrm{H}] = \frac{Y(\pi^+ {}^3\mathrm{H})}{Y(\pi^+ p)} \frac{J_t}{J_p} \frac{N({}^1\mathrm{H})}{N({}^3\mathrm{H})} \{\sigma(\theta)[\pi^+ p]\}_{\mathrm{PWA}} , \quad (7)$$

where J_t is the Jacobian of the pion for $\pi^+ {}^3\mathrm{H}$ scattering and J_p for $\pi^+ p$. The systematic error is mainly due to uncertainties in the absolute $\pi^+ p$ calibration, which is

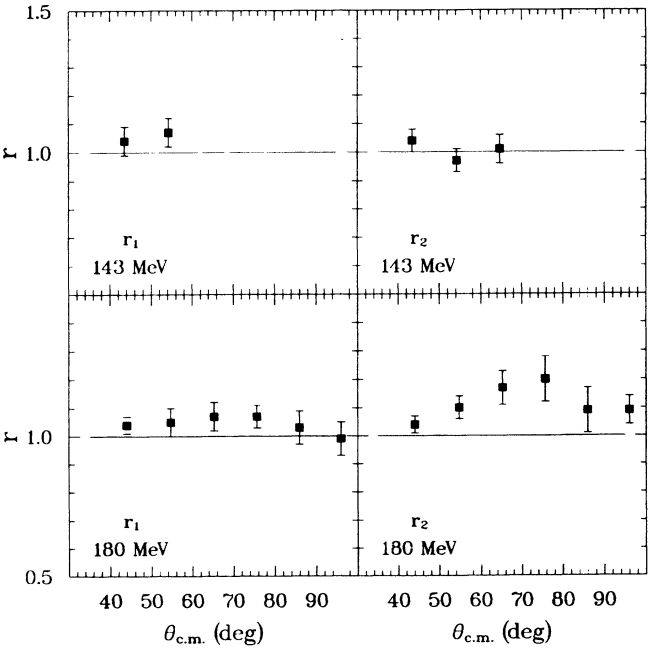

FIG. 3. The "simple" ratios at $T_\pi = 143$ and 180 MeV. The solid line at $r = 1$ indicates the expected value when CS is valid. $r_1 = \sigma(\theta)[\pi^+ \mathrm{H}]/\sigma(\theta)[\pi^- {}^3\mathrm{He}]$, $r_2 = \sigma(\theta)[\pi^- {}^3\mathrm{H}]/\sigma(\theta)[\pi^+ {}^3\mathrm{He}]$.

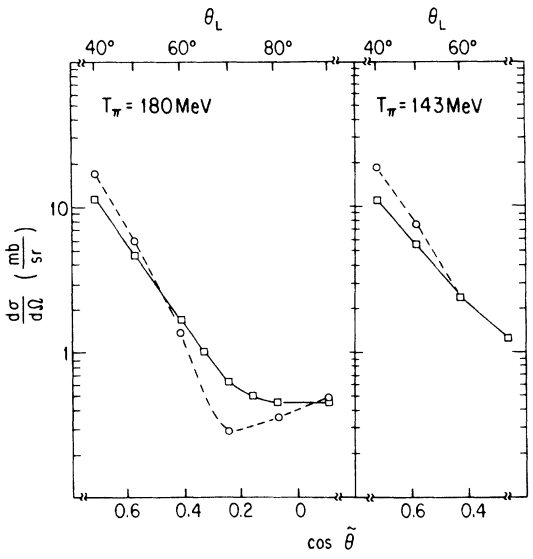

FIG. 4. Cross sections for π^+ ^{3}H elastic scattering indicated by squares and for π^- ^{3}H indicated by circles at $T_\pi = 143$ and 180 MeV. The lines are to guide the eye only. The solid line is π^+ ^{3}H and the dashed line is π^- ^{3}He.

±4%. The cross section for π^+ elastic scattering on ^{3}He has been obtained using the relation

$$\sigma(\theta)[\pi^+ {}^3\mathrm{He}\to\pi^+ {}^3\mathrm{He}] = \frac{\sigma(\theta)[\pi^+ {}^3\mathrm{H}\to\pi^+ {}^3\mathrm{H}]}{\rho_+} \ . \tag{8a}$$

The analogous expression to Eq. (7), in which π^+ is replaced by π^-, was used to evaluate the π^--tritium elastic scattering cross section; we estimate the systematic error to be ±5%. The π^- ^{3}He cross section is obtained using the relation

$$\sigma(\theta)[\pi^- {}^3\mathrm{He}\to\pi^- {}^3\mathrm{He}] = \frac{\sigma(\theta)[\pi^- {}^3\mathrm{H}\to\pi^- {}^3\mathrm{H}]}{\rho_-} \ , \tag{8b}$$

the systematic error is also ±5%.

The differential cross sections for $\pi^\pm$ elastic scattering on ^{3}H/^{3}He are shown in Fig. 4 and given in Table IV. The results will be discussed in the next section.

The results of our pion-deuterium elastic scattering measurements obtained with the deuterium target are given in Table V together with the data reported by the Swiss Institute for Nuclear Research (SIN) group.[17] The agreement between the two sets of data is good. The SIN data at 143 MeV are in good accord with the LAMPF data by Masterson *et al.*[18]

TABLE V. Differential cross sections for $\pi^\pm d\to\pi^\pm d$ compared with SIN data, Ref. 17.

T_π MeV	θ_π lab	$d\sigma/d\Omega$ (lab) in mb/sr This expt. $\pi^+ d\to\pi^+ d$	This expt. $\pi^- d\to\pi^- d$	SIN $\pi^+ d\to\pi^+ d$
143	40°	11.7±0.5	10.2±0.5	9.59±0.48
143	50°	5.16±0.25	5.15±0.25	4.93±0.25
143	60°	2.67±0.13		2.55±0.15
180	40°	10.9±0.5	10.9±0.5	10.5±0.5
180	50°	4.9±0.4	5.26±0.26	4.90±0.26
180	60°	2.26±0.12		1.96±0.10

IV. ANALYSIS

A complete treatment of pion-tritium elastic scattering that fully takes into account absorption, distortion, Δ

TABLE IV. The differential cross section in c.m. for π^+ and π^- elastic scattering on ^{3}H and ^{3}He. The errors are statistical only and do not include a ±4% uncertainly in the π^+ beam calibration and ±5% in π^-.

θ_{lab} (±1.7°)	$\theta_{c.m.}$	$-t$ fm^{-2}	$\sigma(\theta)[\pi^+ {}^3\mathrm{H}]$ mb/sr	$\sigma(\theta)[\pi^- {}^3\mathrm{H}]$ mb/sr	$\sigma(\theta)[\pi^+ {}^3\mathrm{He}]$ mb/sr	$\sigma(\theta)[\pi^- {}^3\mathrm{He}]$ mb/sr
			At $T_\pi = 180$ MeV			
40°	44.0°	0.97	11.7±0.3	17.6±0.4	17.0±0.4	11.3±0.3
50°	54.7°	1.46	4.7±0.2	5.9±0.2	5.4±0.2	5.5±0.2
60°	65.3°	2.01	1.72±0.04	1.46±0.06	1.25±0.04	1.61±0.07
65°	70.5°	2.26	1.03±0.05		0.49±0.03	
70°	75.7°	2.60	0.63±0.02	0.29±0.02	0.24±0.01	0.58±0.01
75°	80.9°	2.90	0.51±0.03		0.22±0.02	
80°	85.9°	3.21	0.45±0.01	0.36±0.02	0.33±0.02	0.44±0.02
90°	96.0°	3.81	0.46±0.02	0.54±0.02	0.49±0.02	0.47±0.02
			At $T_\pi = 143$ MeV			
40°	43.6°	0.70	11.1±0.4	18.4±0.6	17.7±0.6	10.7±0.5
50°	54.2°	1.06	5.5±0.2	7.9±0.6	7.8±0.3	5.4±0.4
60°	64.7°	1.46	2.43±0.10	2.5±0.2	2.39±0.10	
70°	75.1°	1.90	1.25±0.07	0.9±0.1	0.81±0.07	

propagation, and so forth, is not available in relativistic form. There are several potential model calculations, unfortunately, they have not been successful in correctly predicting our data. We have found that the impulse approximation with on-shell πN amplitudes does a credible job in predicting ρ_+ and ρ_- as well as the differential cross sections up to $\theta_{\rm lab} \simeq 75°$. As we will see, despite its obvious shortcomings, the impulse approximation can provide a useful way for probing the cause of CSB in the simple ratios r_1 and r_2 in which many of the correction factors for the approximations of the impulse approximation cancel each other.

A. Pion-tritium elastic scattering

The amplitude for pion-tritium elastic scattering can be written as a sum of a spin-non-flip part, f, and a spin-flip part, g,

$$A(\pi^3\mathrm{H}) = f + i\boldsymbol{\sigma}\cdot\mathbf{n}g \ ,$$

where $\boldsymbol{\sigma}$ is the spin operator and $\mathbf{n}$ is the normal to the scattering plane,

$$\sigma(\theta) = |A|^2 = |f|^2 + |g|^2 \ .$$

We shall use the convenient notation

$$\hat{A} \equiv f + g$$

with the understanding that $|\hat{A}|^2 = |f|^2 + |g|^2$.

In the impulse approximation we have

$$\hat{A}(\pi^3\mathrm{H}) = a_1 F_p [f(\pi p) + g(\pi p)] + 2a_1 F_n [f(\pi n) + g(\pi n)] \ , \tag{9}$$

where $f(\pi p)$ is the pion-proton and $f(\pi n)$ the pion-neutron non-spin-flip elastic scattering amplitude, $g(\pi p)$ is the pion-proton and $g(\pi n)$ the pion-neutron spin-flip amplitude; a_1 is the shadowing factor or medium coefficient; F_p and F_n are the proton and neutron matter form factors of tritium, which are analogous to the electric charge form factor.[19,20]

The tritium nucleus has mainly an s-wave configuration in which the two neutrons have their spin antiparallel

$$|^3\mathrm{H}\rangle = |p\uparrow, n\uparrow, n\downarrow\rangle \ . \tag{10}$$

As a consequence of this spin structure of ^{3}H, pion-neutron scattering with single-neutron spin flip cannot occur. Thus,

$$\hat{A}(\pi^3\mathrm{H}) = a_1 F_p [f(\pi p) + g(\pi p)] + 2a_1 F_n f(\pi n) \ . \tag{11}$$

If charge symmetry in the basic πN scattering reactions is valid, the following relations hold:

$$f(\pi^+ p) = f(\pi^- n) \ , \tag{12a}$$

$$g(\pi^+ p) = g(\pi^- n) \ , \tag{12b}$$

$$f(\pi^- p) = f(\pi^+ n) \ , \tag{12c}$$

$$g(\pi^- p) = g(\pi^+ n) \ . \tag{12d}$$

There is evidence originating from $\pi^\pm d$ scattering experiments[21,22] that CSB in the basic πN systems is less than a few percent. We shall assume for the moment that CS in πN elastic scattering is valid and thus that Eq. (12) applies. This will enable us to evaluate in a transparent way the sensitivity of the charge-symmetry ratios to the differences in the neutron and proton form factors of ^{3}H and ^{3}He.

At $T_\pi = 180$ MeV and throughout the region of the Δ resonance, the following relation is observed:

$$\sigma(\theta)[\pi^+ p \to \pi^+ p] \simeq 9\sigma(\theta)[\pi^- p \to \pi^- p] \ .$$

Thus, we have the *approximate* amplitude relations

$$3f(\pi^- p) \simeq f(\pi^+ p) \equiv \tilde{f} \ , \tag{13a}$$

$$3g(\pi^- p) \simeq g(\pi^+ p) \equiv \tilde{g} \ . \tag{13b}$$

Substitution of Eqs. (12) and (13) into (11) yields

$$\hat{A}(\pi^+ {}^3\mathrm{H}) = a_+ \tilde{f}(F_p + \tfrac{2}{3}F_n) + a_+ \tilde{g} F_p \ , \tag{14a}$$

$$\hat{A}(\pi^- {}^3\mathrm{H}) = a_- \tilde{f}(\tfrac{1}{3}F_p + 2F_n) + \tfrac{1}{3}a_- \tilde{g} F_p \ . \tag{14b}$$

a_+ is the nuclear medium coefficient for π^+ in ^{3}H and a_- for π^- in ^{3}H.

In the momentum transfer region of this experiment, $-1\ \mathrm{fm}^{-2} > t > -4\ \mathrm{fm}^{-2}$, the form factors are expected to be simple exponential functions that only depend on $-t$, $F_n \simeq e^{-\beta_1 t}$, and $F_p \simeq e^{-\beta_2 t}$. Therefore,

$$F_n / F_p \equiv \alpha_t \simeq [1 + (\beta_2 - \beta_1)t]$$

or

$$F_n(^3\mathrm{H}) = \alpha_t F_p(^3\mathrm{H}) \ . \tag{15}$$

This simplifies Eq. (14) to

$$\hat{A}(\pi^+ {}^3\mathrm{H}) = a_+ F_p(^3\mathrm{H})[(1 + \tfrac{2}{3}\alpha_t)\tilde{f} + \tilde{g}] \ , \tag{16a}$$

$$\hat{A}(\pi^- {}^3\mathrm{H}) = a_- F_p(^3\mathrm{H})[(\tfrac{1}{3} + 2\alpha_t)\tilde{f} + \tfrac{1}{3}\tilde{g}] \ . \tag{16b}$$

The cross sections in this notation are

$$\sigma(\theta)[\pi^+ {}^3\mathrm{H}] = a_+^2 |F_p(^3\mathrm{H})|^2 [|(1 + \tfrac{2}{3}\alpha_t)\tilde{f}|^2 + |\tilde{g}|^2] \ , \tag{17a}$$

$$\sigma(\theta)[\pi^- {}^3\mathrm{H}] = a_-^2 |F_p(^3\mathrm{H})|^2 [|(\tfrac{1}{3} + 2\alpha_t)\tilde{f}|^2 + \tfrac{1}{9}|\tilde{g}|^2] \ . \tag{17b}$$

The final simplification which we can make is based on the p-wave approximation to πN scattering in the region of the Δ resonance

$$\tilde{f} \sim 2\cos\theta \ , \tag{18a}$$

$$\tilde{g} \sim \sin\theta \ . \tag{18b}$$

This useful approximation underestimates $\sigma(\theta)[\pi^- {}^3\mathrm{H}]$ somewhat at 90° because of the neglect of s-wave πN scattering. To include the latter, one could change Eq. (18a) to

$$\tilde{f} \sim 2\cos\theta + \varepsilon \ , \tag{18c}$$

ε is small, typically 0.05. The substitution of Eqs. (18a) and (18b) into (17) yields

$$\sigma(\theta)[\pi^+ {}^3\mathrm{H}] \sim a_+^2 |F_p({}^3\mathrm{H})|^2 [(1+\tfrac{2}{3}\alpha_t)^2 4\cos^2\theta + \sin^2\theta] \ , \tag{19a}$$

$$\sigma(\theta)[\pi^- {}^3\mathrm{H}] \sim a_-^2 |F_p({}^3\mathrm{H})|^2 [(\tfrac{1}{3}+2\alpha_t)^2 4\cos^2\theta + \tfrac{1}{9}\sin^2\theta] \ . \tag{19b}$$

At 90° in the πN system, $\sigma(\theta)[\pi^- {}^3\mathrm{H}]$ is small because of the factor $\frac{1}{9}$ in front of $\sin^2\theta$. This implies a dip in the angular distribution for π^3H elastic scattering centered at $\theta(\pi p)=90°$ which corresponds to about 78° in the π^3H c.m. system; this is the non-spin-flip dip. In $\sigma(\theta)[\pi^+ {}^3\mathrm{H}]$ the spin-flip contribution is appreciable and the dip is filled, see Fig. 4.

The result of the calculation of $\sigma(\theta)[\pi^- {}^3\mathrm{H}]$ based on Eq. (17a) is shown in Fig. 5; the calculational particulars are relegated to Appendix A. The agreement with the experimental data is excellent up to ~75°(lab). We conclude from this that the impulse approximation is valid for elastic pion ^{3}H scattering up to about 75°; the angular range agrees with the limits derived from simple kinematic considerations given in Appendix B.

The main features of π^+ and π^- elastic scattering on tritium may be summarized as follows.

(a) In the angular region $\theta_{\mathrm{lab}} \leq 60°$ and $\theta_{\mathrm{lab}} \geq 90°$, one finds that $\sigma(\theta)[\pi^- {}^3\mathrm{H}]$ is larger than $\sigma(\theta)[\pi^+ {}^3\mathrm{H}]$ because the dominant contribution to the cross section comes from f, the (πN) non-spin-flip amplitude.

(b) In the region of the NSF dip $60° < \theta_{\mathrm{lab}} < 90°$, the opposite holds and $\sigma(\theta)[\pi^+ {}^3\mathrm{H}]$ is larger than $\sigma(\theta)[\pi^- {}^3\mathrm{H}]$ because of the dominance of g, the (πN) spin-flip amplitude.

(c) Both $\sigma(\theta)[\pi^+ {}^3\mathrm{H}]$ and $\sigma(\theta)[\pi^- {}^3\mathrm{H}]$ decrease nearly exponentially with increasing angle up to $\theta_{\mathrm{lab}} \simeq 75°$, see Fig. 4. This fall off is due in large measure to the exponential decrease with increasing magnitude of t of the matter form factor, also seen in electron scattering,[12,13] and to the decrease in $f(\pi N)$.

B. Form factors

It is worthwhile to compare $\pi^+ {}^3\mathrm{H}$ elastic scattering directly with $\pi^- {}^3\mathrm{H}$. The ratio, P, of the cross sections is shown in Fig. 6, where

$$P({}^3\mathrm{H}) \equiv \frac{\sigma(\theta)[\pi^- {}^3\mathrm{H} \to \pi^- {}^3\mathrm{H}]}{\sigma(\theta)[\pi^+ {}^3\mathrm{H} \to \pi^+ {}^3\mathrm{H}]} \ . \tag{20}$$

One can substitute Eq. (17) in this equation and make the simplifying assumption that all variables are real numbers. Furthermore, Eq. (18) implies that

$$g/f \simeq \tfrac{1}{2}\tan\theta \ , \tag{21}$$

where θ is the angle in the (πN) system. This yields

$$P({}^3\mathrm{H}) \simeq \frac{a_-^2 (\frac{1}{3}+2\alpha_t)^2 + \frac{1}{9}\frac{1}{4}\tan^2\theta}{a_+^2 (1+\frac{2}{3}\alpha_t)^2 + \frac{1}{4}\tan^2\theta} \ . \tag{22}$$

We have $a_-^2/a_+^2 = 0.9$ for the effect of nuclear shadow-

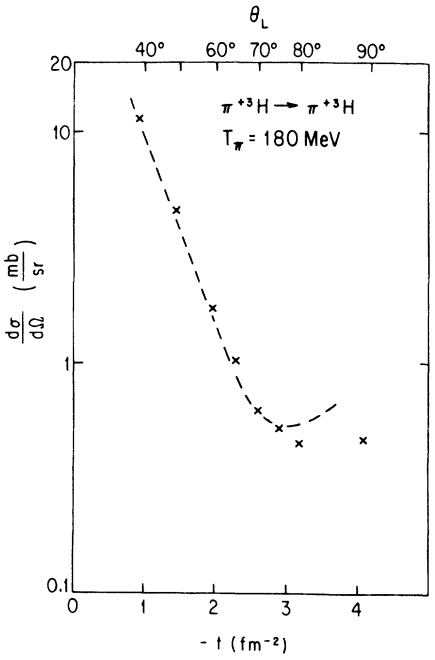

FIG. 5. Comparison of the $d\sigma/d\Omega$ calculation for $\pi^+ {}^3\mathrm{H}$ elastic scattering with our data. The calculation is based on the impulse approximation, Eq. (17) and Appendix A.

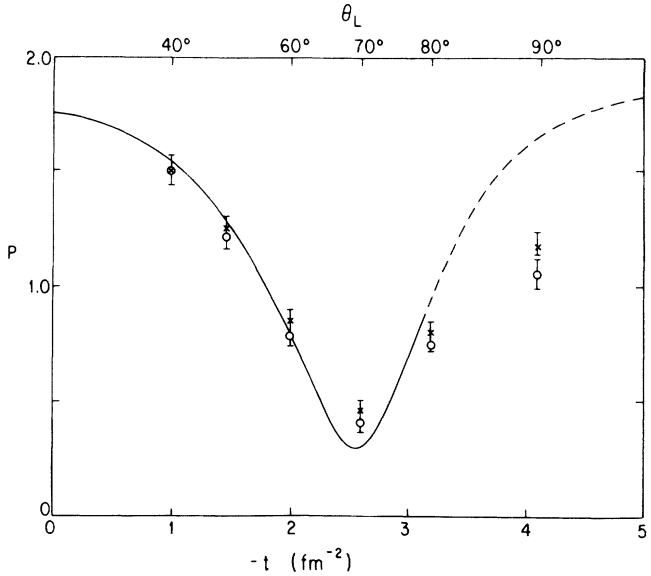

FIG. 6. Comparison of $\pi^+ {}^3\mathrm{H}$ with $\pi^- {}^3\mathrm{H}$ cross sections and $\pi^- {}^3\mathrm{He}$ with $\pi^+ {}^3\mathrm{He}$. The crosses show $P({}^3\mathrm{H}) = \sigma(\theta)[\pi^- {}^3\mathrm{H}]/\sigma(\theta)[\pi^+ {}^3\mathrm{H}]$, and the circles show $P({}^3\mathrm{He}) = \sigma(\theta)[\pi^+ {}^3\mathrm{He}]/\sigma(\theta)[\pi^- {}^3\mathrm{He}]$. The solid line is a calculation based on Eqs. (17a) and (17b) with $\alpha = 1$. The dashed line indicates where the impulse approximation that underlies Eq. (17) breaks down.

ing, see Appendix A. At $\theta=0°$, α_t must be one, therefore,

$$P(^3\mathrm{H})[\text{at } \theta=0°]=0.9\times(\tfrac{7}{5})^2=1.75 \ .$$

At 180° for the case $\alpha_t \geq 1$, we have

$$P(^3\mathrm{H})[\text{at } \theta=180°]\geq 1.75 \ .$$

At $\theta_{\text{c.m.}}(\pi N)=90°$, Eq. (22) becomes

$$P(^3\mathrm{H})[\text{at } \theta_{\text{c.m.}}(\pi N)=90°]=0.9\times\tfrac{1}{9}=0.1 \ .$$

The inclusion of s-wave πN scattering, which is readily done using existing πN PWA data,[16] rather than Eq. (18), yields the value

$$P(^3\mathrm{H})[\text{at } \theta(\pi N)=90°]\simeq 0.3 \ ,$$

which is close to the experimental value. We see from Eq. (22) and Fig. 6 that there is a strong minimum in

$$P(^3\mathrm{H})[\text{at } \theta_{\text{c.m.}}(\pi N)=90°] \ ,$$

which is 78° in the (π^3H) system. This minimum is a reflection of the NSF dip that characterizes the $\pi^-\,^3$H angular distribution.

Note that $P(^3\mathrm{H})$ does not depend on the absolute value of the proton and neutron matter form factors, only on their ratio $\alpha_t=F_n(^3\mathrm{H})/F_p(^3\mathrm{H})$. The solid line in Fig. 6 shows our calculation of $P(^3\mathrm{H})$ using Eq. (17) with $\alpha_t=1$. The agreement with the data is excellent up to about 75° in the lab which is the limit of the applicability of the impulse approximation with on-shell kinematics, see Appendix B. The calculation from 80° on is indicated by a dashed line as it has not been adjusted for the shortcomings of the impulse approximation.

It is of interest to compare $P(^3\mathrm{H})$ with

$$P(^3\mathrm{He})\equiv\frac{\sigma(\theta)[\pi^+\,^3\mathrm{He}\rightarrow\pi^+\,^3\mathrm{He}]}{\sigma(\theta)[\pi^-\,^3\mathrm{He}\rightarrow\pi^-\,^3\mathrm{He}]} \ . \tag{23}$$

The data are shown by circles in Fig. 6. The P function is a very sensitive way for comparing the ratio of neutron and proton form factors in ^{3}H and ^{3}He since $P(^3\mathrm{H})$ is a function of

$$\alpha_t(^3\mathrm{H})=F_n(^3\mathrm{H})/F_p(^3\mathrm{H}) \ ,$$

while $P(^3\mathrm{He})$ is governed by

$$\alpha_t(^3\mathrm{He})=F_p(^3\mathrm{He})/F_n(^3\mathrm{He}) \ .$$

This is discussed in Appendix C. We see from Fig. 6 that $P(^3\mathrm{H})\simeq P(^3\mathrm{He})$ to about 10% at all angles. The accuracy of comparing $\alpha_t(^3\mathrm{H})$ and $\alpha_t(^3\mathrm{He})$ in this experiment is limited by the uncertainty in the calibration of the $\pi^\pm$ beam fluxes.

In the region of the ($\pi^-\,^3$H) NSF dip, the $\pi^+\,^3$H cross section is relatively large because the (π^+p) spin-flip amplitude is significant. In this region Eq. (19a) reduces to

$$\sigma(\theta)[\pi^+\,^3\mathrm{H}]=a_+^2[|g(\pi^+p)|^2+s]|F_p(^3\mathrm{H})|^2 \tag{24}$$

where s is a small correction for the s-wave contribution that has been neglected in Eq. (18a). Equation (24) provides a golden opportunity for a determination of the proton matter form factor of tritium. The substitution of our ($\pi^+\,^3$H) cross section data at $T_\pi=180$ MeV at $\theta_{\text{lab}}=70°$ (or $t=-2.6\ \text{fm}^{-2}$) yields

$$|F_p(^3\mathrm{H})|^2=0.07\pm0.02 \ , \tag{25}$$

see Ref. 15. For comparison, note that the electromagnetic form factors at the same t, Ref. 14, are $|F_m(^3\mathrm{H})|^2=0.10$ and $|F_c(^3\mathrm{H})^2=0.09$.

We recapitulate the physics of Eq. (24). In the region of the NSF dip, the cross section is dominated by the spin-flip amplitude on the odd nucleon as a consequence of the spin structure of ^{3}H and the Pauli principle. The only nucleon available for a spin flip is the proton in ^{3}H. Thus, $\sigma(\theta)[\pi^+\,^3\mathrm{H}]$ is governed by $\sigma(\theta)[\pi^+p]$ and by the value of the proton form factor. A detailed treatment of the intricacies of the matter form factor determination will be given elsewhere (Ref. 23).

C. Charge symmetry

The isomirror relations of Eq. (17) are

$$\sigma(\theta)[\pi^-\,^3\mathrm{He}]=a_-^2(^3\mathrm{He})|F_n(^3\mathrm{He})|^2\{[1+\tfrac{2}{3}\alpha_t(^3\mathrm{He})]\tilde{f}|^2+|\tilde{g}|^2\} \ , \tag{26a}$$

$$\sigma(\theta)[\pi^+\,^3\mathrm{He}]=a_+^2(^3\mathrm{He})F_n(^3\mathrm{He})|^2\{|[\tfrac{1}{3}+2\alpha_t(^3\mathrm{He})]\tilde{f}|^2+\tfrac{1}{9}|\tilde{g}|^2\} \ , \tag{26b}$$

the definition for $\alpha_t(^3\mathrm{He})$ is analogous to $\alpha_t(^3\mathrm{H})$, Eq. (15),

$$F_p(^3\mathrm{He})\equiv\alpha_t(^3\mathrm{He})F_n(^3\mathrm{He})$$

$$\simeq[1+(\beta_2'-\beta_1')t]F_n(^3\mathrm{He}) \ .$$

In the region of the NSF dip where $f\ll 1$, it follows from Eqs. (17a) and (26a), that the charge-symmetry simple ratio r_1 is given by

$$r_1\simeq\left|\frac{g(\pi^+p)}{g(\pi^-n)}\right|^2\cdot\left|\frac{F_p(^3\mathrm{H})}{F_n(^3\mathrm{He})}\right|^2 \ , \tag{27}$$

where we have used $a_+(^3\mathrm{H})\simeq a_-(^3\mathrm{He})$, see Appendix A.

In Ref. 21 the following data are reported, $\sigma(\theta)[\pi^+d]\simeq(1.01\pm0.01)\sigma(\theta)[\pi^-d]$ near $\theta(\pi d)=90°$. We estimate from this and the expression for $A(\pi d)$ that is analogous to Eq. (9)

$$g(\pi^+p)=(1.01\pm0.01)g(\pi^-n) \ , \tag{28}$$

in the region of the NSF dip, barring accidental cancellations. Thus, the r_1 data near $t=-2.6$ fm^{-2} imply

$$F_p(^3\mathrm{H})=(1.03\pm0.04)F_n(^3\mathrm{He})\ . \tag{29}$$

This result means that there is little or no CSB here. We have, therefore, that near $t=-2.6$ fm^{-2} the proton matter form factor of ^{3}H is the same within 4% than the neutron form factor of ^{3}He.

Next we consider the charge-symmetry ratio r_2, Eq. (1b) and Fig. 3(b). In the region of the NSF dip, the $\pi^-\,^3$H cross section is small and depends on a combination of F_p and F_n. There is no simple interpretation like Eq. (27) for r_1. Outside the NSF dip, for $\theta\leq 60°$, $\sigma(\theta)[\pi^-\,^3\mathrm{H}]$ is dominated by $(\pi^- n)$ non-spin-flip scattering on the *paired neutrons* and we can write, using $a_-(^3\mathrm{H})=a_+(^3\mathrm{He})$,

$$r_2\simeq\left|\frac{f(\pi^- n)}{f(\pi^+ p)}\right|^2\cdot\left|\frac{2F_n(^3\mathrm{H})+\frac{1}{3}F_p(^3\mathrm{H})}{2F_p(^3\mathrm{He})+\frac{1}{3}F_n(^3\mathrm{He})}\right|^2\ . \tag{30}$$

To the extent that $2F_n(^3\mathrm{H})\geq\frac{1}{3}F_p(^3\mathrm{H})$, and $2F_p(^3\mathrm{He})\geq\frac{1}{3}F_n(^3\mathrm{He})$, we can simplify this to

$$r_2\simeq\left|\frac{F_n(^3\mathrm{H})}{F_p(^3\mathrm{He})}\right|^2\ , \tag{31}$$

where we have also used $f(\pi^- n)=f(\pi^+ p)$ based on the near equality of the $\pi^+ d$ and $\pi^- d$ data of Ref. 21. Thus, deviations in r_2 from 1.0 are due mainly to the difference in the form factors of the paired nucleons. Our data are consistent with

$$F_n(^3\mathrm{H})=[1+(0.03\pm0.02)|t|]F_p(^3\mathrm{He})\ . \tag{32}$$

From the experimentalist's standpoint, the cleanest and most convincing test of CS is the superratio, R, Eq. (2) and Fig. 2. To interpret the observed deviation of R from 1.0, we could substitute Eqs. (17) and (26) into Eq. (2). There are then three parameters that must be adjusted,

$$\alpha_t(^3\mathrm{H})=F_n(^3\mathrm{H})/F_p(^3\mathrm{H})\ ,$$

$$\alpha_t(^3\mathrm{He})=F_p(^3\mathrm{He})/F_n(^3\mathrm{He})\ ,$$

and finally the ratio $F_p(^3\mathrm{H})/F_n(^3\mathrm{He})$ which is also a function of t. This three-parameter fit is the subject of a separate paper. Our data on the superratio are consistent with the previously listed values

$$F_p(^3\mathrm{H})=(1.03\pm0.04)F_n(^3\mathrm{He})$$

and

$$F_n(^3\mathrm{H})=[1+(0.03\pm0.02)|t|]F_p(^3\mathrm{He})\ .$$

D. Model calculations

There is a large variety of model calculations of $\pi^{\pm}\,^3$H elastic scattering. We intend to review them in a forthcoming publication in which additional measurements[24] at other energies and angles are analyzed as well.[25] It is fair to say in advance, that, in general, the agreement with the data is poor. We shall limit this section to two model calculations of the superratio and simple ratios.

(a) Barshay and Sehgal[26] (BS) have used an impulse-approximation-type calculation with an *ad hoc* geometrical model for ^{3}H and ^{3}He with exponential matter form factors. They ascribe the deviation of the superratio from 1.0 to the existence of short-range three-nucleon correlations. Their prediction for the cross sections at $T_\pi=180$ MeV is shown in Fig. 7 and for the ratios in Fig. 8. There is a large discrepancy with our data, especially for $\sigma(\theta)[\pi^-\,^3\mathrm{H}]$ in the region of the NSF dip. This is due in part because BS neglect s-wave πN scattering; they use Eq. (18a) instead of Eq. (18c). These discrepancies render the BS discussion of possible CSB effects useless and their evaluation of the differences in the ^{3}H and ^{3}He form factors.

Kim, Kim, and Landau (KKL), Ref. 27, have employed the LPOTT program based on a momentum space, nonlocal potential with many theoretical parameters to provide an improved description for off-energy-shell, recoil, binding, and kinematic effects, featuring spin-flip scattering that takes into account the spin structure of ^{3}H. The agreement of the calculated cross sections with our data viewed on a log scale (see Fig. 7) is good, but there are some important differences on close inspection. This is perhaps not so surprising as the authors used 20-year-old πN phase shifts. The KKL prediction for the charge-symmetry ratios is shown in Fig. 8. Particularly striking is the disagreement in R and r_2 at $\theta_{\mathrm{c.m.}}=44°$, 54.7°, and 65.5°. We conclude that despite substantial efforts there does not exist a theoretical description that can account for our ratio data that uses Coulomb modifications to an otherwise charge-symmetric potential. The violation of CS observed in Figs. 2 and 3 is not purely of electromagnetic origin but it has a nuclear component as well.

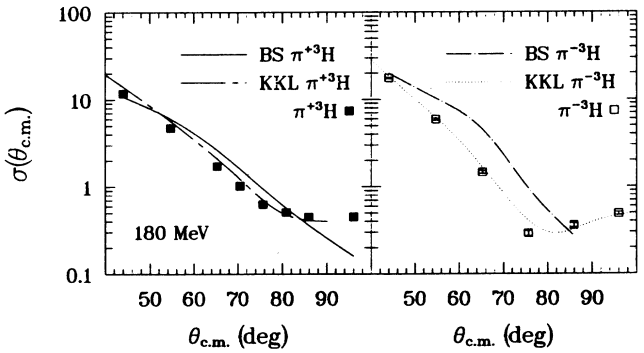

FIG. 7. Comparison of our $\sigma(\theta)[\pi^{\pm}\,^3\mathrm{H}]$ results with the cross-section calculation of Barshay and Sehgal (BS), Ref. 26 and of Kim, Kim, and Landau (KKL), Ref. 27.

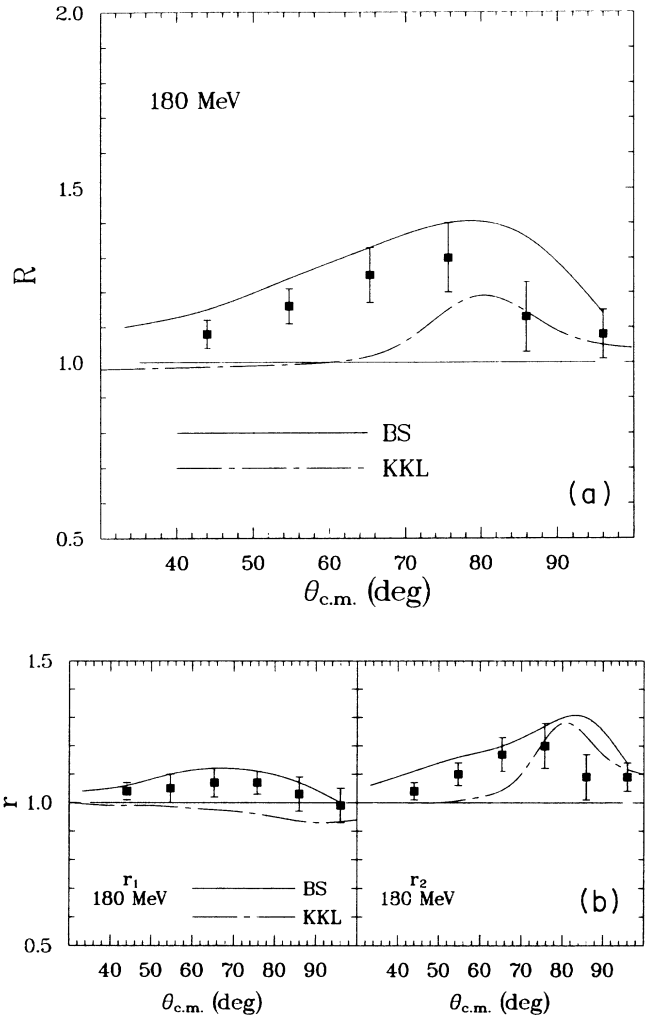

FIG. 8. Comparison of predictions by BS (Ref. 26) and KKL (Ref. 27) of the superratio R and the charge-symmetry ratios r_1 and r_2 with our data.

V. COULOMB CORRECTIONS

Electromagnetic interactions are not invariant under the CS operation; they give rise to a potentially important limit to our test of CS. There are various different em effects.

(1) Bremsstrahlung. This process can be evaluated in a convenient way using the external emission dominance hypothesis.[28] The effect on R, r_1, and r_2 is less than 1%.

(2) Pure Coulomb scattering. The Coulomb amplitude A_c is inversely proportional to t,

$$A_c = -2\eta\bar{p}F_\pi F_A/t \ ,$$

where $\eta = Q(\pi^\pm)Ze^2$ and $Q(\pi^\pm)$ is the electric charge of the pion, Z is the electric charge of the target nucleus (^{3}H or ^{3}He), F_π is the pion form factor, and F_A is the charge form factor of ^{3}H or ^{3}He. At $\theta_{lab}=40°$, we have $\sigma(\theta)_c = |A_c|^2 = 0.2\ \mu$b/sr or 0.1% of $\sigma(\theta)_N[\pi^+ {}^3\mathrm{H}]$.

(3) Coulomb nuclear interference. The contribution to the cross section is

$$\Delta\sigma_{in} = 2A_f A_c \cos\phi \ ,$$

where ϕ is the phase between the Coulomb amplitude A_c and the nuclear non-spin-flip amplitude A_f. The effect on the ratios is $<2\%$.

(4) Coulomb barrier differences for inelastic channels

$$\sigma(\theta)[\pi^+ {}^3\mathrm{He}\to\pi^+ npp] \neq \sigma(\theta)[\pi^- {}^3\mathrm{H}\to\pi^- pnn] \ .$$

The correction of this to the ratios is less than 1%.

(5) Coulomb distortion of the nuclear Hamiltonian. At our energies we expect this to be small.

(6) The most serious electromagnetic correction is due to the shift in effective interaction energy, E_c, where

$$E_c = Q(\pi)Z(^3A)e^2/R = 1.4Z \text{ MeV fm}/R \ ,$$

where R is the interaction distance between pion and nucleus. We estimate that $E_c = \pm 0.8$ MeV for $\pi^\pm {}^3$H scattering and double that for $\pi^\pm {}^3$He. The consequence of this energy shift is opposite for r_1 and r_2 and it cancels mostly for R. More data on the energy dependence of the $\pi^\pm {}^3$H and $\pi^\pm {}^3$He elastic scattering are needed for a detailed evaluation. We estimate the effect on r_1 and r_2 to be less than 4%.

VI. CONCLUSION

Measurements of the charge-symmetry ratios for $\pi^\pm$ elastic scattering on ^{3}H and ^{3}He at $T_\pi = 180$ MeV from $\theta_{lab}=40°$ to 90° and at $T_\pi = 143$ MeV from $\theta_{lab}=40°$ to 60° indicate that $r_2 > 1.0$ and $R > 1.0$ which is a clear violation of CS. The cause for this is a small difference in the form factors of the paired nucleon

$$F_n(^3\mathrm{H}) = [1+(0.03\pm0.01)|t|]F_p(^3\mathrm{He}) \ .$$

The form factors of the odd nucleon do not indicate a violation outside error since r_1 is consistent with one

$$F_p(^3\mathrm{H}) = (1.03\pm0.04)F_n(^3\mathrm{He}) \ .$$

The angular distribution for $\pi^+ {}^3$H elastic scattering decreases monotonically with increasing pion angle up to 80°; the slope is related to the charge form factor slope. $\sigma(\theta)[\pi^- {}^3\mathrm{H}]$ decreases in similar fashion with increasing angle but it falls off more rapidly near $\theta_{lab}=70°$ to generate a dip, the so-called NSF dip.

Note added. A very interesting analysis of our charge-symmetry superratio and simple ratio data has been made recently by Gibbs and Gibson.[30] Using standard multiple scattering analysis techniques, they find that the difference between the even radii of ^{3}H and ^{3}He is

$$r_n(^3\mathrm{H}) - r_p(^3\mathrm{He}) = -0.030\pm0.008 \text{ fm}$$

and between the odd radii

$$r_p(^3\mathrm{H}) - r_n(^3\mathrm{He}) = -0.035\pm0.007 \text{ fm} \ .$$

This indicates a violation of charge symmetry in the wave function. The accuracy claimed for the difference in the radii is much higher than the accuracy of the electromagnetic radii which are known to ± 0.040 fm.[12,13]

ACKNOWLEDGMENTS

It is a pleasure to acknowledge the invaluable contribution made by J. VanDyke in designing and testing the pressurized tritium gas target and by H. Maltrud in filling and emptying the gas targets and performing the gas analysis. The responsibility for the tritium safety procedures rested with T. Putnam and D. Cochran. The assistance of R. Boudrie and C. Morris in setting up the EPICS spectrometer and J. Holt in the analysis are much appreciated. This work was supported in part by the U.S. Department of Energy (DOE).

APPENDIX A: THE π^3H CROSS SECTION IN THE IMPULSE APPROXIMATION

The calculation of the π^+ ^{3}H cross section shown by the dashed line in Fig. 5 is based on Eq. (17). The proton matter form factor of ^{3}H is taken to be equal to the charge form factor at the same value of t (Ref. 14). Neutron and proton form factors are chosen to be equal, or $\alpha_t = 1$. For f and g, we used the on-shell spin-non-flip and spin-flip $\pi^+ p$ scattering amplitudes given by the VPI πN PWA (Ref. 16) at $T_\pi = 180$ MeV. The angle transformation for going from the πN to the π^3H system is simple when using as a variable the Lorentz invariant four momentum transfer, t, instead of the angle θ, it is just the ratio of the π^3H to πN Jacobians. We estimate the nuclear shadowing factors to be $a_+(^3\text{H}) = a_-(^3\text{He}) = 0.86$ and $a_-(^3\text{H}) = a_+(^3\text{He}) = 0.82$ based on measurements of $\sigma_t(\pi d)$ and $\sigma_t(\pi^4\text{He})$ (Refs. 22 and 29); these values are consistent with black-sphere scattering.

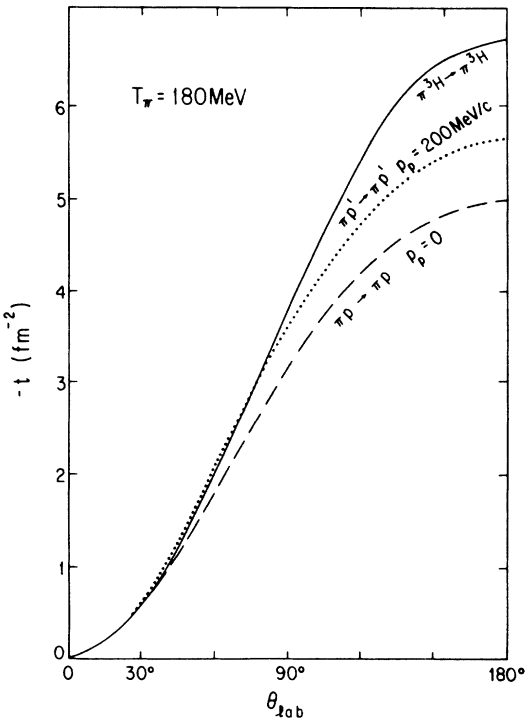

FIG. 9. Kinematics of πp and π^3H elastic scattering, specifically, the dependence of t on θ_{lab} at $T_\pi = 180$ MeV. The solid line is for π^3H elastic scattering, the dashed line for πp with the proton at rest; the dotted line is for πp with the proton moving toward the incident pion with a momentum of 200 MeV/c.

APPENDIX B: THE LIMIT OF THE IMPULSE APPROXIMATION

The kinematics of πp and π^3H elastic scattering are shown in Fig. 9. Specifically, the value of t is given as a function of the pion laboratory scattering angle θ_{lab}. The maximum possible $|t|$ for πN scattering is 5 fm^{-2} corresponding to 110° (lab) in the π^3H system. For larger scattering angles, the single scattering approximation must be modified by the inclusion of off-shell effects and multiple interactions. Actually, at every angle, $|t|$ for the πN system is always less than $|t|$ for the π^3H system. Scattering can still take place because of Fermi momentum which modifies the $t - \theta_{\text{lab}}$ relation. An example is shown in Fig. 9 by the dotted line which is the $t - \theta_{\text{lab}}$ relation for πN scattering when the nucleon is off shell, it is not at rest but moves towards the pion with a momentum of 200 MeV/c. This suggests that up to $\theta_{\text{lab}} \sim 75°$ there is no problem with using the impulse approximation.

APPENDIX C: THE SUPERQUOTIENT OR THE RATIO OF THE NEUTRON AND PROTON FORM FACTORS OF ^{3}H and ^{3}He

Charge symmetry implies that at every four-momentum transfer

$$F_n(^3\text{H}) = F_p(^3\text{He})$$

and

$$F_p(^3\text{H}) = F_n(^3\text{He}) .$$

Consider the following ratio of elastic scattering cross sections which we want to name the superquotient:

$$Q = \frac{\sigma(\theta)[\pi^- {}^3\text{H}]}{\sigma(\theta)[\pi^+ {}^3\text{H}]} \times \frac{\sigma(\theta)[\pi^- {}^3\text{He}]}{\sigma(\theta)[\pi^+ {}^3\text{He}]} = \frac{P(^3\text{H})}{P(^3\text{He})} = \frac{r_2}{r_1} . \tag{C1}$$

CS implies that $Q = 1.0$ at every energy and angle. Outside the NSF dip region where $f > g$, we can simplify Eq. (C1) using Eqs. (17) and (26) as follows:

$$Q = \left| \frac{\frac{1}{3} + 2\alpha_t(^3\text{H})}{\frac{1}{3} + 2\alpha_t(^3\text{He})} \right|^2 \times \left| \frac{1 + \frac{2}{3}\alpha_t(^3\text{He})}{1 + \frac{2}{3}\alpha_t(^3\text{H})} \right|^2 , \tag{C2}$$

we have also used $a_+(^3\text{H}) = a_-(^3\text{He})$ and $a_-(^3\text{H}) = a_+(^3\text{He})$.

Let us apply this to the special case where $\alpha_t(^3\text{H}) = 1$ and where $\alpha_t(^3\text{He})$ is similar to $\alpha_t(^3\text{H})$ so we can write

$$\alpha_t(^3\text{He}) = (1 + \delta_t)\alpha_t(^3\text{H}) . \tag{C3}$$

Substitution into Eq. (C2) yields the value $Q \simeq 1-0.9\delta_t$. Experimentally, we have at $T_\pi = 180$ MeV at $\theta_{\rm lab} = 90°$, which corresponds to $t = -3$ fm^2, that $Q = 1.10 \pm 0.08$, thus $\delta_{t=-3} = -0.11 \pm 0.09$, or

$$\frac{F_n(^3\mathrm{H})}{F_p(^3\mathrm{H})} = (0.89 \pm 0.09)\frac{F_p(^3\mathrm{He})}{F_n(^3\mathrm{He})} \ . \tag{C4}$$

This is, of course, another way for saying that CS is violated. Figure 6 indicates that $P(^3\mathrm{H}) > P(^3\mathrm{He})$, or $Q > 1.0$, at all angles except at $t = -1$ fm^{-2} where there is no difference. Thus, using the superquotient Q we see evidence for CSB also. The advantage of the superratio as discussed in Sec. IV is the great experimental accuracy because of the cancellation of the π^+ and π^- beam calibrations and detection efficiencies. The disadvantage of the superquotient is that the systematic error depends on the square of the π^-/π^+ beam calibration. The advantages of Q are that uncertainties in the ratio of the ^{3}H/^{3}He gas pressures cancel and that there is a simple interpretation of Q in terms of the ratio of the four matter form factors.

---

*Present address: Department of Physics, George Washington University, Washington, D.C. 20052.
†Deceased.
‡Present address: Los Alamos National Laboratory, Los Alamos, NM 87545.
§Present address: Department of Physics, Texas A&M University, College Station, TX 77843 and Texas Accelerator Center, The Woodlands, TX 77380.

[1] *Isospin in Nuclear Physics,* edited by D. H. Wilkinson (North-Holland, Amsterdam, 1969).
[2] G. A. Miller, B. M. K. Nefkens, and I. Slaus, Phys. Rep. (in press).
[3] E. M. Henley and G. A. Miller, in *Mesons in Nuclei,* edited by M. Rho and D. Wilkinson (North-Holland, Amsterdam, 1979), Vol. 1.
[4] S. Weinberg, *Festschrift for I. I. Rabi* (New York Academy of Science, New York, 1977).
[5] D. J. Gross, S. B. Treiman, and F. Wilczek, Phys. Rev. D **19**, 2188 (1979).
[6] A. W. Thomas, P. Bickerstaff, and A. Gersten, Phys. Rev. D **24**, 2539 (1981).
[7] B. M. K. Nefkens, W. J. Briscoe, A. D. Eichon, D. H. Fitzgerald, J. A. Holt, A. A. Mokhtari, J. A. Wightman, M. E. Sadler, R. Boudrie, and C. Morris, Phys. Rev. Lett. **52**, 735 (1984).
[8] I. Slaus, Y. Akaishi, and H. Tanaka, Phys. Rev. Lett. **48**, 993 (1982).
[9] J. L. Friar, B. F. Gibson, and G. L. Payne, Comments Nucl. Part. Phys. **11**, 51 (1983).
[10] B. M. K. Nefkens and I. Slaus, *Few-Body Systems* (Springer-Verlag, New York, 1987), Suppl. 2, p. 432.
[11] B. M. K. Nefkens, in *Few Body Systems and Nuclear Forces II,* Vol. 87 of *Lecture Notes in Physics,* edited by H. Zingl *et al.* (Springer-Verlag, New York, 1978), p. 189.
[12] F. P. Juster *et al.*, Phys. Rev. Lett. **55**, 2261 (1985).
[13] D. Beck *et al.*, Phys. Rev. Lett. **59**, 1537 (1987).
[14] D. Beck, Ph.D. thesis, Massachusetts Institute of Technology, 1980 (unpublished).
[15] B. M. K. Nefkens, in *Lecture Notes in Physics* (Springer-Verlag, New York, 1986), Vol. 260, p. 364.
[16] R. A. Arndt, J. M. Ford, and L. D. Roper, Phys. Rev. D **32**, 1085 (1985), and update reported in Proceedings of Physics with Light Mesons and The Second International Workshop on πN Physics, edited by W. R. Gibbs and B. M. K. Nefkens, LANL Report LA-11184-C, 1987.
[17] K. Gabathuler *et al.*, Nucl. Phys. **A350**, 253 (1980).
[18] T. G. Masterson, J. J. Kraushaar, R. J. Peterson, R. S. Raymond, R. A. Ristinen, R. L. Boudrie, E. F. Gibson, and A. W. Thomas, Phys. Rev. C **26**, 2091 (1982).
[19] B. F. Gibson, Phys. Rev. **139B**, 1153 (1965).
[20] R. Landau, Ann. Phys. (NY) **92**, 205 (1975).
[21] G. Smith *et al.*, Phys. Rev. C **38**, 240 (1988).
[22] E. Pedroni *et al.*, Nucl. Phys. **A300**, 321 (1978).
[23] B. M. K. Nefkens (unpublished).
[24] C. Pillai, D. B. Barlow, B. L. Berman, W. J. Briscoe, A. Mokhtari, B. M. K. Nefkens, A. M. Petrov, and M. E. Sadler, Phys. Lett. B **207**, 389 (1988).
[25] C. Pillai, D. B. Barlow, B. L. Berman, W. J. Briscoe, A. Mokhtari, B. M. K. Nefkens, and M. E. Sadler (unpublished).
[26] S. Barshay and L. M. Sehgal, Phys. Rev. C **31**, 2133 (1985).
[27] Kr. T. Kim, Y. E. Kim, and R. H. Landau, Phys. Rev. C **36**, 2155 (1987).
[28] B. M. K. Nefkens and D. I. Sober, Phys. Rev. D **14**, 2434 (1976).
[29] C. Wilkin, C. R. Cox, J. J. Domingo, K. Gabathuler, E. Pedroni, J. Rohlin, P. Schwaller, and N. W. Tanner, Nucl. Phys. **B62**, 61 (1973).
[30] W. R. Gibbs and B. F. Gibson, LANL Report LA-UR-89-4181, 1989 (submitted to Phys. Rev. C).